Scattering from dielectric frequency selective structures

Forslund, Ola; Karlsson, Anders; Poulsen, Sören

2001

CODEN:LUTEDX/(TEAT-7101)/1-23/(2001)

Scattering from dielectric frequency selective structures

Ola Forslund, Anders Karlsson, and Sören Poulsen

Department of Electroscience
Electromagnetic Theory
Lund Institute of Technology
Sweden

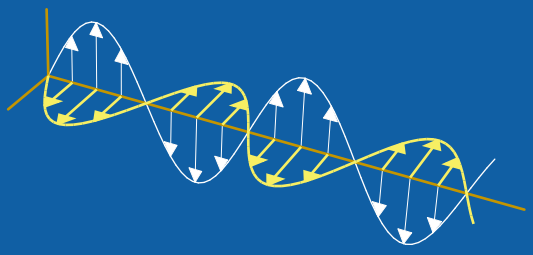

Ola Forslund

Department of Electromagnetic Theory
Royal Institute of Technology
SE-100 44 Stockholm
Sweden

Anders Karlsson (Anders.Karlsson@es.lth.se)

Department of Electroscience
Electromagnetic Theory
Lund Institute of Technology
P.O. Box 118
SE-221 00 Lund
Sweden

Sören Poulsen (Soren.Poulsen@acab.se)

Applied Composites AB
P.O. Box 163
SE-341 23 Ljungby
Sweden

Editor: Gerhard Kristensson

Abstract

A plane wave impinges on a laterally double-periodic inhomogeneous lossy dielectric structure. Using a wave splitting approach, and an expansion of the fields and permittivity in global and local basis functions, respectively, the scattered fields are determined via a propagator. The formulation is useful for a permittivity which varies abruptly as well as in a continuous fashion. A subdomain basis for the constitutive parameter is preferred to an entire domain basis. Calculated results are compared with experimental data for a slab with domains of a piecewise homogeneous permittivity. The agreement is good considering the error sources in the experiment. The results are in a special case also compared with results obtained by an entirely different method showing very good agreement. The method is also used on a pyramidal absorber-like structure.

1 Introduction

Frequency selective surfaces (FSS) have been used in antennas and radomes throughout several decades [5–7]. The application areas are mainly filtering (with respect to frequency and angle) and scanning. A conventional frequency selective surface usually consists of one or more thin screens of periodically distributed metallic patches or apertures in a ground plane. The thin screens are stacked and separated by homogeneous sheets of dielectric material. Much effort, theoretical and experimental, has been spent to increase the understanding and to develop efficient computation models for such structures. The computational times involved in the analysis of a conventional FSS is highly dependent upon finding efficient basis functions for the conducting elements. Some recent developments have been reported in [8]. Experience from decades of research in the topic of conventional FSS has been summarized in [3]. When considering metal screens made from commercially available etched metal clad laminates, a model assuming an infinitely thin perfectly conducting (PEC) screen is often adequate at microwave and millimetre wave frequencies. It is sometimes of interest though, to consider a screen with a thickness. Such PEC screens have been analyzed in [1, 2]. Recently, comparisons between models assuming an infinitely thin screen and a screen with a small thickness have been performed in [9].

In this paper another type of frequency selective structure is considered: a dielectric slab with 2D-periodic variation of the permittivity in the lateral direction and arbitrary variation in a longitudinal z-direction. This structure is hereafter denoted a *dielectric frequency selective structure*. In the analysis performed here, it is assumed that the object does not contain any PEC:s although it could be combined with a conventional metallic screen. This paper concentrates on providing an analysis method for the structures described. The numerical performance of the approach is illustrated for some simple geometries.

Gratings and doubly periodic structures have been analyzed with other methods than the one described here. In [10, 11] e.g. , FEM was used for the interior domain in combination with a boundary integral equation. Inhomogeneous dielectric gratings

that are periodic in one direction have been analyzed by Forslund and He [12, 13]. In [13] they used a Green's function approach based on a vacuum wave-splitting to solve the scattering problem; the paper includes calculated examples for arbitrary incidence and continuously inhomogeneous media. In [14] a similar approach was used but for the total tangential fields; the analysis was restricted to incidence in the principal plane and the examples to piecewise homogeneous domains. In papers [13, 14] the analysis also comprised bianisotropic media. Earlier, dielectric gratings with piecewise homogeneous subdomains and 1D-variation have been analyzed and elaborated upon in e.g. [16, 17].

The mechanism causing the frequency selectivity in a dielectric frequency selective structure is in general different from that of a conventional FSS. Stacked thin metallic screens separated by homogeneous dielectrics (typically in the order of $\lambda/4$) can be designed to act as filters for the fundamental mode only, although for a sparse grid or at higher frequencies, higher order modes can be excited within the supporting slabs. Dielectric frequency selective structures obtain their selectivity from higher order modes excited in the slab. These modes interfere destructively and constructively with the fundamental mode. Unlike a conventional FSS, a dielectric frequency selective structure with finite conductivity can never be designed to obtain a bandpass response; a bandstop response can however be obtained. At high frequencies these structures are highly dependent on the angle of incidence. At frequencies considerably lower than cut off, the dielectric structure acts as a homogenized non-isotropic material for the fundamental mode; the material can under these conditions be represented by an effective permittivity tensor. Homogenized materials and gratings have been analyzed in [19, 20]. As frequency increases the higher order modes first become surface wave modes that are bound to the slab and then, at higher frequencies, they start to propagate in free space, i.e. they become grating lobes.

2 Theory

2.1 Problem formulation

In this paper, a dielectric structure that is periodic in two directions is considered. In the longitudinal direction the structure occupies the region $0 \leq z \leq \ell$. It is assumed to be isotropic, lossy, and non-magnetic ($\mu = 1$). The complex relative permittivity $\varepsilon = \varepsilon' + i\varepsilon''$ of the slab is periodic such that

$$\varepsilon(\boldsymbol{r}_t, z) = \varepsilon(\boldsymbol{r}_t + \boldsymbol{d}_1, z) = \varepsilon(\boldsymbol{r}_t + \boldsymbol{d}_2, z), \quad 0 \leq z \leq \ell$$

where $\boldsymbol{r}_t = x\hat{x} + y\hat{y}$ and $\boldsymbol{d}_1$ and $\boldsymbol{d}_2$ are two vectors that span the xy-plane, cf. Figure 1, but are not necessarily orthogonal. Without loss of generality it is assumed to be vacuum outside the slab.

In most cases an incident plane wave is of interest. However, in the case of a cascade of several periodic structures the incident field for each structure is a sum of Floquet modes, due to this the incident field in this paper is assumed to be a

general sum of Floquet modes. The derivation in the following sections comprises the following steps: definition of an orthonormal set of vector basis functions on the cell considered; expansion of the fields in the inhomogeneous and in the homogeneous regions, respectively; expansion of the permittivity in local- and entire domain basis functions, respectively; insertion of the expansions in the Maxwell equations; derivation of a set of coupled ODE:s through the use of orthogonality relations; definition of a propagator; solution of the ODE for the propagator; calculation of the reflection- and transmission matrices by a wave splitting technique.

2.2 Vector basis functions

In order to represent the fields and the material of the problem, a suitable set of basis functions is chosen. A time dependence $\mathrm{e}^{-i\omega t}$ is adopted. A scalar function $Q(\boldsymbol{r}_t, z)$ that is periodic on the closed domain $\mathcal{I}$ defined in Figure 1 can on every z-plane be expanded in the complete orthonormal basis

$$\begin{array}{l} \eta_{mn}(\boldsymbol{r}_t) = D^{-1/2}\,\mathrm{e}^{i\boldsymbol{k}_{f;mn}\cdot\boldsymbol{r}_t} \quad \text{where} \\ \boldsymbol{k}_{f;mn} = \frac{2\pi}{D}\,(m\,\hat{z}\times\boldsymbol{d}_1 - n\,\hat{z}\times\boldsymbol{d}_2) \quad \text{and} \\ D = |\boldsymbol{d}_1\times\boldsymbol{d}_2| \end{array} \tag{2.1}$$

see e.g. [1], D is the area of the cell and $\boldsymbol{r} = \boldsymbol{r}_t + z\hat{z}$. The fields are pseudoperiodic when a plane wave is incident. A pseudoperiodic function

$$Q'(\boldsymbol{r}_t, z) = Q(\boldsymbol{r}_t, z)\,\mathrm{e}^{i\boldsymbol{k}_t\cdot\boldsymbol{r}_t} \tag{2.2}$$

where $Q(\boldsymbol{r}_t, z)$ is periodic and where

$$\boldsymbol{k}_t = k_0\sin(\theta_0)\,(\cos(\varphi_0)\,\hat{x} + \sin(\varphi_0)\,\hat{y}) \tag{2.3}$$

can be expanded in the complete orthonormal set

$$\psi_{mn}(\boldsymbol{r}_t) = \eta_{mn}(\boldsymbol{r}_t)\,\mathrm{e}^{i\boldsymbol{k}_t\cdot\boldsymbol{r}_t} = D^{-1/2}\,\mathrm{e}^{i\boldsymbol{k}_{t;mn}\cdot\boldsymbol{r}_t} \tag{2.4}$$

where $\boldsymbol{k}_{t;mn} = \boldsymbol{k}_t + \boldsymbol{k}_{f;mn}$ and $m = \ldots, -1, 0, 1\ldots$ and $n = \ldots, -1, 0, 1\ldots$. The functions in the electromagetic case are vector valued and hence a complete set of orthonormal vector functions are required. A set of orthonormal vector functions are defined as

$$\begin{array}{l} \boldsymbol{A}_{1mn}(\boldsymbol{r}_t) = k_{t;mn}^{-1}\nabla\psi_{mn}(\boldsymbol{r}_t)\times\hat{z} = i\psi_{mn}(\boldsymbol{r}_t)\,\hat{k}_{t;mn}\times\hat{z} \\ \boldsymbol{A}_{2mn}(\boldsymbol{r}_t) = k_{t;mn}^{-1}\nabla\psi_{mn}(\boldsymbol{r}_t) = i\psi_{mn}(\boldsymbol{r}_t)\,\hat{k}_{t;mn} \\ \boldsymbol{A}_{3mn}(\boldsymbol{r}_t) = \psi_{mn}(\boldsymbol{r}_t)\hat{z} \end{array} \tag{2.5}$$

where $\hat{k}_{t;mn} = \boldsymbol{k}_{t;mn}/|\boldsymbol{k}_{t;mn}|$ and $k_{t;mn} = |\boldsymbol{k}_{t;mn}|$. These vector functions satisfy a number of properties, see Appendix A. It is convenient to introduce

$$\boldsymbol{k}_{z;mn} = k_{z;mn}\hat{z} = \hat{z}\begin{cases} (k_0^2 - |\boldsymbol{k}_{t;mn}|^2)^{1/2} & \text{when} \quad k_0 \geq |\boldsymbol{k}_{t;mn}| \\ i(|\boldsymbol{k}_{t;mn}|^2 - k_0^2)^{1/2} & \text{when} \quad k_0 < |\boldsymbol{k}_{t;mn}| \end{cases} \tag{2.6}$$

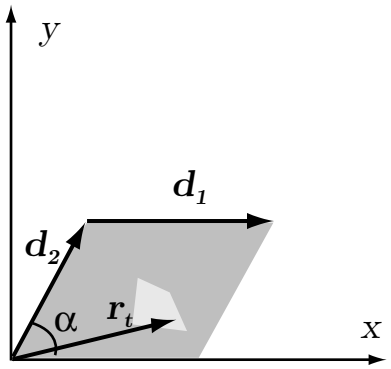

Figure 1: The periodically repeating cell.

The following normalized quantities are also introduced

$$\gamma_{mn} = \frac{k_{z;mn}}{k_0}$$
$$\lambda_{mn} = \frac{k_{t;mn}}{k_0}$$

A set of normalized vector wave functions are defined as

$$\begin{aligned}
\boldsymbol{u}_{1mn}(\boldsymbol{r}) &= \mathrm{e}^{i\gamma_{mn}k_0 z}\boldsymbol{A}_{1mn}(\boldsymbol{r}_t) = \hat{u}_{\perp mn}(\boldsymbol{r}_t)\ \mathrm{e}^{i\gamma_{mn}k_0 z} \\
\boldsymbol{u}_{2mn}(\boldsymbol{r}) &= \frac{1}{k_0}\nabla\times\left(\mathrm{e}^{i\gamma_{mn}k_0 z}\boldsymbol{A}_{1mn}(\boldsymbol{r}_t)\right) = \hat{u}_{\parallel mn}(\boldsymbol{r}_t)\ \mathrm{e}^{i\gamma_{mn}k_0 z} \\
\boldsymbol{v}_{1mn}(\boldsymbol{r}) &= \mathrm{e}^{-i\gamma_{mn}k_0 z}\boldsymbol{A}_{1mn}(\boldsymbol{r}_t) = \hat{v}_{\perp mn}(\boldsymbol{r}_t)\ \mathrm{e}^{-i\gamma_{mn}k_0 z} \\
\boldsymbol{v}_{2mn}(\boldsymbol{r}) &= -\frac{1}{k_0}\nabla\times\left(\mathrm{e}^{-i\gamma_{mn}k_0 z}\boldsymbol{A}_{1mn}(\boldsymbol{r}_t)\right) = \hat{v}_{\parallel mn}(\boldsymbol{r}_t)\ \mathrm{e}^{-i\gamma_{mn}k_0 z}.
\end{aligned} \tag{2.7}$$

These functions are divergence free and satisfy the free space vector Helmholtz equation

$$\nabla\times\left(\nabla\times\boldsymbol{u}_{\tau mn}(\boldsymbol{r})\right) - k_0^2\boldsymbol{u}_{\tau mn}(\boldsymbol{r}) = -\nabla^2\boldsymbol{u}_{\tau mn}(\boldsymbol{r}) - k_0^2\boldsymbol{u}_{\tau mn}(\boldsymbol{r}) = 0.$$

The functions $\boldsymbol{u}_{\tau mn}(\boldsymbol{r})$ correspond to forward traveling waves ($+z$ direction) and $\boldsymbol{v}_{\tau mn}(\boldsymbol{r})$ to backward traveling waves.

2.3 Derivation of ODE for quantities proportional to the tangential $\boldsymbol{E}$ and $\boldsymbol{H}$ fields

In this section, the chosen set of basis functions is used to represent the fields. The expressions for the fields are substituted into the Maxwell equations and a system of ODE:s for the slab considered is obtained. In the inhomogeneous region as well

as in free space the following expansion is made

$$\begin{aligned}\boldsymbol{E}(\boldsymbol{r}) &= \sum_{mn}\big\{g_{1mn}(k_0z)\boldsymbol{A}_{1mn}(\boldsymbol{r}_t) + k_0^{-1}\nabla\times g_{2mn}(k_0z)\boldsymbol{A}_{1mn}(\boldsymbol{r}_t)\\ &\qquad + g_{3mn}(k_0z)\boldsymbol{A}_{3mn}(\boldsymbol{r}_t)\big\}\\ &= \sum_{mn}\big\{g_{1mn}(k_0z)\boldsymbol{A}_{1mn}(\boldsymbol{r}_t) + g'_{2mn}(k_0z)\boldsymbol{A}_{2mn}(\boldsymbol{r}_t)\\ &\qquad + \big(\lambda_{mn}g_{2mn}(k_0z) + g_{3mn}(k_0z)\big)\boldsymbol{A}_{3mn}(\boldsymbol{r}_t)\big\}.\end{aligned} \tag{2.8}$$

Prime denotes differentiation with respect to k_0z where k_0 is the vacuum wave number. Note that the third term, $g_{3mn}(k_0z)\boldsymbol{A}_{3mn}(\boldsymbol{r}_t)$ is the only term that is not divergence free. In free space $g_{3mn}(k_0z)$ equals zero. The magnetic field is divergence free and is expanded as

$$\begin{aligned}i\eta_0\boldsymbol{H}(\boldsymbol{r}) &= \sum_{mn}\big\{h_{1mn}(k_0z)\boldsymbol{A}_{1mn}(\boldsymbol{r}_t) + k_0^{-1}\nabla\times\big(h_{2mn}(k_0z)\boldsymbol{A}_{1mn}(\boldsymbol{r}_t)\big\}\\ &= \sum_{mn}\big\{h_{1mn}(k_0z)\boldsymbol{A}_{1mn}(\boldsymbol{r}_t) + h'_{2mn}(k_0z)\boldsymbol{A}_{2mn}(\boldsymbol{r}_t)\\ &\qquad + \lambda_{mn}h_{2mn}(k_0z)\boldsymbol{A}_{3mn}(\boldsymbol{r}_t)\big\}.\end{aligned} \tag{2.9}$$

From the Maxwell equations, a system of linear ODE:s are obtained for the expansion coefficients. The curl of the electric field reads

$$\begin{aligned}\nabla\times\boldsymbol{E}(\boldsymbol{r}) = k_0\sum_{mn}\big\{&\big(\lambda_{mn}^2g_{2mn}(k_0z) - g''_{2mn}(k_0z) + \lambda_{mn}g_{3mn}(k_0z)\big)\boldsymbol{A}_{1mn}(\boldsymbol{r}_t)\\ &+g'_{1mn}(k_0z)\boldsymbol{A}_{2mn}(\boldsymbol{r}_t) + \lambda_{mn}g_{1mn}(k_0z)\boldsymbol{A}_{3mn}(\boldsymbol{r}_t)\big\}.\end{aligned}$$

The curl of the magnetic field reads

$$\begin{aligned}\nabla\times\boldsymbol{H}(\boldsymbol{r}) = -\frac{i}{\eta_0}k_0\sum_{mn}\big\{&\big(\lambda_{mn}^2h_{2mn}(k_0z) - h''_{2mn}(k_0z)\big)\boldsymbol{A}_{1mn}(\boldsymbol{r}_t)\\ &+ h'_{1mn}(k_0z)\boldsymbol{A}_{2mn}(\boldsymbol{r}_t) + \lambda_{mn}h_{1mn}(k_0z)\boldsymbol{A}_{3mn}(\boldsymbol{r}_t)\big\}.\end{aligned}$$

The induction law and the orthogonality relation (A.1) gives

$$\begin{aligned}h_{1mn}(k_0z) &= -g''_{2mn}(k_0z) + \lambda_{mn}^2g_{2mn}(k_0z) + \lambda_{mn}g_{3mn}(k_0z)\\ h_{2mn}(k_0z) &= g_{1mn}(k_0z).\end{aligned} \tag{2.10}$$

Ampere's law gives

$$\begin{aligned}&\sum_{mn}\big\{\big(\lambda_{mn}^2g_{1mn}(k_0z) - g''_{1mn}(k_0z)\big)\boldsymbol{A}_{1mn}(\boldsymbol{r}_t) + h'_{1mn}(k_0z)\boldsymbol{A}_{2mn}(\boldsymbol{r}_t)\\ &\qquad + \lambda_{mn}h_{1mn}(k_0z)\boldsymbol{A}_{3mn}(\boldsymbol{r}_t)\big\}\\ &\quad = \varepsilon(\boldsymbol{r})\sum_{mn}\big\{g_{1mn}(k_0z)\boldsymbol{A}_{1mn}(\boldsymbol{r}_t) + g'_{2mn}(k_0z)\boldsymbol{A}_{2mn}(\boldsymbol{r}_t)\\ &\qquad + \lambda_{mn}^{-1}\big(g''_{2mn}(k_0z) + h_{1mn}(k_0z)\big)\boldsymbol{A}_{3mn}(\boldsymbol{r}_t)\big\}.\end{aligned} \tag{2.11}$$

where Eq. (2.10) has been used. From Eq. (2.11) three ODE:s are obtained for $g_{1mn}(k_0 z)$, $h_{1mn}(k_0 z)$ and $h'_{2mn}(k_0 z)$. In order to obtain a system of four first order ODE:s, $g'_{1mn}(k_0 z)$ is also introduced as an independent function. The two first equations are obtained by multiplying Eq. (2.11) by in turn $\boldsymbol{A}^*_{1mn}(\boldsymbol{r}_t)$ and $\boldsymbol{A}^*_{2mn}(\boldsymbol{r}_t)$ and using the orthogonality. The third equation is obtained by multiplying Eq. (2.11) by $\varepsilon(\boldsymbol{r})^{-1}\boldsymbol{A}^*_{3mn}(\boldsymbol{r}_t)$ and using the orthogonality. The fourth equation is simply the identity $\partial_z h_{2mn}(k_0 z) = k_0 h'_{2mn}(k_0 z)$. A rearranged version of the system of equations then reads

$$\frac{\partial}{\partial k_0 z}\begin{pmatrix} h_{1mn}(k_0 z) \\ g'_{2mn}(k_0 z) \\ g_{1mn}(k_0 z) \\ h'_{2mn}(k_0 z) \end{pmatrix} = \mathcal{D}_{mn}\begin{pmatrix} h_{1mn}(k_0 z) \\ g'_{2mn}(k_0 z) \\ g_{1mn}(k_0 z) \\ h'_{2mn}(k_0 z) \end{pmatrix} + \sum_{m'n'} \mathcal{C}_{mn,m'n'}\begin{pmatrix} h_{1m'n'}(k_0 z) \\ g'_{2m'n'}(k_0 z) \\ g_{1m'n'}(k_0 z) \\ h'_{2m'n'}(k_0 z) \end{pmatrix} \tag{2.12}$$

where the matrix $\mathcal{D}$ is given by

$$\mathcal{D}_{mn} = \begin{pmatrix} 0 & 1 & 0 & 0 \\ -\gamma_{mn}^2 & 0 & 0 & 0 \\ 0 & 0 & 0 & 1 \\ 0 & 0 & -\gamma_{mn}^2 & 0 \end{pmatrix}$$

and the matrix $\mathcal{C}$ by

$$\mathcal{C}_{mn,m'n'} = \begin{pmatrix} 0 & \alpha_{12} & \alpha_{13} & 0 \\ \alpha_{21} & 0 & 0 & 0 \\ 0 & 0 & 0 & 0 \\ 0 & \alpha_{42} & \alpha_{43} & 0 \end{pmatrix}.$$

Note that the unknowns in (2.12) are all proportional to the tangential field components. The coefficients α read

$$\begin{aligned}
\alpha_{12} &= \int_{\text{cell}} (\varepsilon(\boldsymbol{r}) - 1)\boldsymbol{A}^*_{2mn}(\boldsymbol{r}_t) \cdot \boldsymbol{A}_{2m'n'}(\boldsymbol{r}_t)\, dS \\
\alpha_{13} &= \int_{\text{cell}} \varepsilon(\boldsymbol{r})\boldsymbol{A}^*_{2mn}(\boldsymbol{r}_t) \cdot \boldsymbol{A}_{1m'n'}(\boldsymbol{r}_t)\, dS \\
\alpha_{21} &= \lambda_{mn}\lambda_{m'n'} \int_{\text{cell}} \left((\varepsilon(\boldsymbol{r}))^{-1} - 1\right) \boldsymbol{A}^*_{3mn}(\boldsymbol{r}_t) \cdot \boldsymbol{A}_{3m'n'}(\boldsymbol{r}_t)\, dS \\
\alpha_{42} &= \alpha_{13} = -\int_{\text{cell}} \varepsilon(\boldsymbol{r})\boldsymbol{A}^*_{1mn}(\boldsymbol{r}_t) \cdot \boldsymbol{A}_{2m'n'}(\boldsymbol{r}_t)\, dS \\
\alpha_{43} &= -\alpha_{12} = -\int_{\text{cell}} (\varepsilon(\boldsymbol{r}) - 1)\, \boldsymbol{A}^*_{1mn}(\boldsymbol{r}_t) \cdot \boldsymbol{A}_{1m'n'}(\boldsymbol{r}_t)\, dS.
\end{aligned} \tag{2.13}$$

It is worthwhile to make the numerical calculation of the matrix $\mathcal{C}_{mn,m'n'}$ as efficient as possible, since it is the most time-consuming calculation in the numerical algorithm. There are several different ways to do the calculation. A straightforward numerical integration is not efficient. It is better to expand $\varepsilon(\boldsymbol{r})$ in a suitable set

of basis functions. One possible set is the Floquet mode basis which is a global set over the cell. (See Appendix B.) However, it is often better to use an expansion in local pulse functions u_p such that

$$u_p(\boldsymbol{r}) = \begin{cases} 1 & \text{if} \quad \boldsymbol{r}_t \in \Omega_p \\ 0 & \text{otherwise} \end{cases} \tag{2.14}$$

where e.g. Ω_p is a triangular subdomain of Ω and Ω is a subdomain of the entire cell $\mathcal{I}$. The pulse basis is particularly useful when having a piecewise homogeneous medium. Assuming that the cell consists of two piecewise homogeneous domains where say ε_i is the relative permittivity within a polygon shaped domain Ω and ε_s is the parameter in the complementary domain $\mathcal{I}\backslash\Omega$, then the matrix coefficient α_{12} can be calculated as

$$\alpha_{12} = \delta_{mm'}\delta_{nn'}(\varepsilon_s - 1) + \sum_p (\varepsilon_i - \varepsilon_s) \int_{\Omega_p} \boldsymbol{A}^*_{2mn}(\boldsymbol{r}_t) \cdot \boldsymbol{A}_{2m'n'}(\boldsymbol{r}_t) dS. \tag{2.15}$$

The other matrix coefficients can be calculated in a similar way. In this way, multiply connected domains can easily be treated in a computer code. (Note that for a material with more complicated constitutive relations, the matrix $\mathcal{C}$ will have more elements $\neq 0$.)

2.4 Propagator formulation

In [13] a transmission Green's function approach is used to solve the scattering problem for a medium varying periodically in one dimension. However, a more convenient approach can be obtained by defining a propagator that maps the unknown components h_{1mn}, g'_{2mn}, g_{1mn} and h'_{2mn} from $k_0 z'$ to $k_0 z$. The (+ to −) propagator $\mathcal{K}(k_0 z, k_0 z')$ is defined by

$$\begin{pmatrix} h_{1mn}(k_0 z) \\ g'_{2mn}(k_0 z) \\ g_{1mn}(k_0 z) \\ h'_{2mn}(k_0 z) \end{pmatrix} = \sum_{m'n'} \mathcal{K}_{mn,m'n'}(k_0 z, k_0 z') \begin{pmatrix} h_{1m'n'}(k_0 z') \\ g'_{2m'n'}(k_0 z') \\ g_{2m'n'}(k_0 z') \\ h'_{2m'n'}(k_0 z') \end{pmatrix} \tag{2.16}$$

where $\mathcal{K}_{mn,m'n'}$ is a 4×4 block matrix. Notice that g_{1mn} and g'_{2mn} are the tangential electric mode fields corresponding to TE and TM cases respectively, *cf.* Eq. (2.8). Likewise $h_{1mn}(k_0 z)$ and $h'_{2mn}(k_0 z)$ are components proportional to the tangential magnetic mode fields corresponding to the TM and TE cases respectively, cf Eq. (2.9).

If Eq. (2.16) is inserted into Eq. (2.12) the following differential equation is obtained:

$$\frac{\partial}{\partial k_0 z} \mathcal{K}(k_0 z, k_0 z') = (\mathcal{D} + \mathcal{C}(k_0 z)) \mathcal{K}(k_0 z, k_0 z') \tag{2.17}$$

with boundary condition

$$\mathcal{K}(k_0 z', k_0 z') = I$$

This equation is solved by backward integration from $k_0 z'$ to $k_0 z$. Useful properties of the propagator matrix $\mathcal{K}$ are

$$\mathcal{K}(k_0 z, k_0 z')\mathcal{K}(k_0 z', k_0 z'') = \mathcal{K}(k_0 z, k_0 z'')$$
$$\mathcal{K}(k_0 z, k_0 z')^{-1} = \mathcal{K}(k_0 z', k_0 z).$$

Thus, cascading several slabs is straightforward and no matrix inversions are required to derive the resulting propagator.

2.5 Wave splitting

In [13] wave splitting is adopted before solving the ODE system. Here, vacuum wave splitting is merely used to derive the transmission and reflection matrices for the modes. In vacuum $\varepsilon(\boldsymbol{r}) = 1$ and the system of equations read

$$\frac{\partial}{\partial k_0 z}\begin{pmatrix} h_{1mn}(k_0 z) \\ g'_{2mn}(k_0 z) \\ g_{1mn}(k_0 z) \\ h'_{2mn}(k_0 z) \end{pmatrix} = \mathcal{D}_{mn}\begin{pmatrix} h_{1mn}(k_0 z) \\ g'_{2mn}(k_0 z) \\ g_{1mn}(k_0 z) \\ h'_{2mn}(k_0 z) \end{pmatrix}.$$

This system consists of two subsystems with equal coefficient matrices

$$\frac{\partial}{\partial k_0 z}\begin{pmatrix} h_{1mn}(k_0 z) \\ g'_{2mn}(k_0 z) \end{pmatrix} = \begin{pmatrix} 0 & 1 \\ -\gamma_{mn}^2 & 0 \end{pmatrix}\begin{pmatrix} h_{1mn}(k_0 z) \\ g'_{2mn}(k_0 z) \end{pmatrix}$$

$$\frac{\partial}{\partial k_0 z}\begin{pmatrix} g_{1mn}(k_0 z) \\ h'_{2mn}(k_0 z) \end{pmatrix} = \begin{pmatrix} 0 & 1 \\ -\gamma_{mn}^2 & 0 \end{pmatrix}\begin{pmatrix} g_{1mn}(k_0 z) \\ h'_{2mn}(k_0 z) \end{pmatrix}.$$

The eigenvalues of the matrices are $\pm i\gamma_{mn}$ and two corresponding eigenvectors

$$\begin{pmatrix} 1 \\ i\gamma_{mn} \end{pmatrix} \quad \text{and} \quad \begin{pmatrix} 1 \\ -i\gamma_{mn} \end{pmatrix}.$$

The wave splitting is defined by

$$\begin{pmatrix} v^+_{mn}(k_0 z) \\ v^-_{mn}(k_0 z) \\ w^+_{mn}(k_0 z) \\ w^-_{mn}(k_0 z) \end{pmatrix} = \mathcal{P}_{mn}\begin{pmatrix} h_{1mn}(k_0 z) \\ g'_{2mn}(k_0 z) \\ g_{1mn}(k_0 z) \\ g'_{1mn}(k_0 z) \end{pmatrix}. \tag{2.18}$$

The matrix $\mathcal{P}_{mn}$ is chosen so that that the transmission and reflection matrices can be derived directly from it, which is shown in section 2.6.

$$\mathcal{P}_{mn} = \frac{1}{i2\gamma_{mn}}\begin{pmatrix} i\gamma_{mn} & 1 & 0 & 0 \\ -i\gamma_{mn} & 1 & 0 & 0 \\ 0 & 0 & i\gamma_{mn} & 1 \\ 0 & 0 & i\gamma_{mn} & -1 \end{pmatrix}. \tag{2.19}$$

The inverse is

$$\mathcal{P}_{mn}^{-1} = \begin{pmatrix} 1 & -1 & 0 & 0 \\ i\gamma_{mn} & i\gamma_{mn} & 0 & 0 \\ 0 & 0 & 1 & 1 \\ 0 & 0 & i\gamma_{mn} & -i\gamma_{mn} \end{pmatrix}. \tag{2.20}$$

The ODE system for $v_{mn}^{\pm}(k_0 z)$ and $w_{mn}^{\pm}(k_0 z)$ is then diagonal in free space and has trivial solutions.

2.6 Transmission and reflection matrices

Transmission and reflection coefficients can be defined in different ways. One way is to define these coefficients from the tangential fields. A definition more consistent with most textbooks is to define them with respect the unit vectors $\hat{u}_{\parallel mn}(\boldsymbol{r}_t)$, $\hat{u}_{\perp mn}(\boldsymbol{r}_t)$, $\hat{v}_{\parallel mn}(\boldsymbol{r}_t)$ and $\hat{v}_{\perp mn}(\boldsymbol{r}_t)$ orthogonal to the free space propagation direction of modes mn. Denote by $\boldsymbol{e}_{mn}^{TM+}$, $\boldsymbol{e}_{mn}^{TE+}$, $\boldsymbol{e}_{mn}^{TM-}$ and $\boldsymbol{e}_{mn}^{TE-}$ the forward $(+z)$ and backward propagating electric fields for mode mn in free space. By observing that $v^- = w^- = 0$ for forward, and $v^+ = w^+ = 0$ for backward propagating modes respectively and by using equations (2.8) and (2.18)

$$\begin{aligned}
\boldsymbol{e}_{mn}^{TM+}(\boldsymbol{r}_t, k_0 z) &= v_{mn}^{+}(k_0 z)\big(i\gamma_{mn}\boldsymbol{A}_{2mn}(\boldsymbol{r}_t) + \lambda_{mn}\boldsymbol{A}_{3mn}(\boldsymbol{r}_t)\big) = v_{mn}^{+}(k_0 z)\ \hat{u}_{\parallel mn}(\boldsymbol{r}_t) \\
\boldsymbol{e}_{mn}^{TM-}(\boldsymbol{r}_t, k_0 z) &= v_{mn}^{-}(k_0 z)\big(i\gamma_{mn}\boldsymbol{A}_{2mn}(\boldsymbol{r}_t) - \lambda_{mn}\boldsymbol{A}_{3mn}(\boldsymbol{r}_t)\big) = v_{mn}^{-}(k_0 z)\ \hat{v}_{\parallel mn}(\boldsymbol{r}_t) \\
\boldsymbol{e}_{mn}^{TE+}(\boldsymbol{r}_t, k_0 z) &= w_{mn}^{+}(k_0 z)\boldsymbol{A}_{1mn}(\boldsymbol{r}_t) = w_{mn}^{+}(k_0 z)\ \hat{u}_{\perp mn}(\boldsymbol{r}_t) \\
\boldsymbol{e}_{mn}^{TE-}(\boldsymbol{r}_t, k_0 z) &= w_{mn}^{-}(k_0 z)\boldsymbol{A}_{1mn}(\boldsymbol{r}_t) = w_{mn}^{-}(k_0 z)\ \hat{v}_{\perp mn}(\boldsymbol{r}_t)
\end{aligned} \tag{2.21}$$

is obtained. Thus the components of the splitting defined by (2.18) directly gives the forward and backward propagating TM and TE modes. The modes correspond to physically forward and backward propagating modes in free space. The transmission and reflection matrices are now defined by

$$\begin{pmatrix} v_{mn}^{+}(k_0\ell) \\ w_{mn}^{+}(k_0\ell) \end{pmatrix} = \sum_{m'n'} \mathcal{T}_{mn,m'n'} \begin{pmatrix} v_{m'n'}^{+}(0) \\ w_{m'n'}^{+}(0) \end{pmatrix} \tag{2.22}$$

and

$$\begin{pmatrix} v_{mn}^{-}(0) \\ w_{mn}^{-}(0) \end{pmatrix} = \sum_{m'n'} \Gamma_{mn,m'n'} \begin{pmatrix} v_{m'n'}^{+}(0) \\ w_{m'n'}^{+}(0) \end{pmatrix} \tag{2.23}$$

where $\mathcal{T}_{mn,m'n'}$ and $\Gamma_{mn,m'n'}$ have the 2×2 block structure

$$\mathcal{T}_{mn,m'n'} = \begin{pmatrix} \mathcal{T}_{mn,m'n'}^{TM,TM} & \mathcal{T}_{mn,m'n'}^{TM,TE} \\ \mathcal{T}_{mn,m'n'}^{TE,TM} & \mathcal{T}_{mn,m'n'}^{TE,TE} \end{pmatrix}.$$

Using (2.16) and (2.18)

$$\begin{pmatrix} v_{mn}^{+}(0) \\ v_{mn}^{-}(0) \\ w_{mn}^{+}(0) \\ w_{mn}^{-}(0) \end{pmatrix} = \sum_{m'n'} \mathcal{P}_{mn}\mathcal{K}_{mn,m'n'}(0, k_0\ell)\mathcal{P}_{m'n'}^{-1} \begin{pmatrix} v_{m'n'}^{+}(k_0\ell) \\ v_{m'n'}^{-}(k_0\ell) \\ w_{m'n'}^{+}(k_0\ell) \\ w_{m'n'}^{-}(k_0\ell) \end{pmatrix} \tag{2.24}$$

is obtained. Let

$$\mathcal{G}_{\mathcal{A}mn,m'n'} = \begin{pmatrix} \mathcal{G}_{\mathcal{A}mn,m'n'}^{11} & \mathcal{G}_{\mathcal{A}mn,m'n'}^{12} \\ \mathcal{G}_{\mathcal{A}mn,m'n'}^{21} & \mathcal{G}_{\mathcal{A}mn,m'n'}^{22} \end{pmatrix} \tag{2.25}$$

where

$$\mathcal{G}_{\mathcal{A}mn,m'n'}^{ij} = \left(\mathcal{P}_{mn}\mathcal{K}_{mn,m'n'}(0,k_0\ell)\mathcal{P}_{m'n'}^{-1}\right)^{2i-1,2j-1} \tag{2.26}$$

and where $i = 1, 2$ and $j = 1, 2$. Similarly define $\mathcal{G}_{\mathcal{B}}, \mathcal{G}_{\mathcal{C}}$ and $\mathcal{G}_{\mathcal{D}}$ such that

$$\begin{aligned} \mathcal{G}_{\mathcal{B}}{}_{mn,m'n'}^{ij} &= \left(\mathcal{P}_{mn}\mathcal{K}_{mn,m'n'}(0,k_0\ell)\mathcal{P}_{m'n'}^{-1}\right)^{2i-1,2j} \\ \mathcal{G}_{\mathcal{C}}{}_{mn,m'n'}^{ij} &= \left(\mathcal{P}_{mn}\mathcal{K}_{mn,m'n'}(0,k_0\ell)\mathcal{P}_{m'n'}^{-1}\right)^{2i,2j-1} \\ \mathcal{G}_{\mathcal{D}}{}_{mn,m'n'}^{ij} &= \left(\mathcal{P}_{mn}\mathcal{K}_{mn,m'n'}(0,k_0\ell)\mathcal{P}_{m'n'}^{-1}\right)^{2i,2j}. \end{aligned} \tag{2.27}$$

The transmission matrix follows from equations (2.22), (2.24) and (2.26). Since waves are incident from the $(-)$ side only, $(v^-_{mn}(k_0\ell) = w^-_{mn}(k_0\ell) = 0)$

$$\mathcal{T} = {\mathcal{G}_{\mathcal{A}}}^{-1} \tag{2.28}$$

is obtained. Similarly, the reflection matrix follows from (2.23), (2.24), (2.27) and (2.28)

$$\Gamma = \mathcal{G}_{\mathcal{C}}\ \mathcal{T}. \tag{2.29}$$

Until now it has been assumed that there is vacuum for $z > \ell$. However in the example in section 3.3, the structure is assumed metal-backed. Thus

$$\begin{pmatrix} v^-_{mn}(k_0\ell) \\ w^-_{mn}(k_0\ell) \end{pmatrix} = \sum_{m'n'} -\delta_{mm'}\delta_{nn'} \begin{pmatrix} v^+_{m'n'}(k_0\ell) \\ w^+_{m'n'}(k_0\ell) \end{pmatrix}. \tag{2.30}$$

Hence, in this case the reflection matrix at $z = 0$ is obtained from (2.23), (2.24), (2.26), (2.27) and (2.30) as

$$\Gamma = (\mathcal{G}_{\mathcal{C}} - \mathcal{G}_{\mathcal{D}})(\mathcal{G}_{\mathcal{A}} - \mathcal{G}_{\mathcal{B}})^{-1}. \tag{2.31}$$

3 Numerical examples

3.1 Slab with circular holes

In this example a homogeneous slab with circular holes is considered. The cell parameters are: $d_1 = d_2 = 22.5$ mm, $\alpha = 90°$. The slab slab thickness is 5.1 mm, and the hole radius 7.5 mm and the permittivity of the slab $\varepsilon = 3.97 + i0.037$. Floquet modes with indices $|m|, |n| \leq 5$ are included. The permittivity is represented in the pulse basis (2.14).

In Figure 2, showing the magnitude of the transmission, the results calculated by the method of the authors is compared with results obtained with a commercial

code MAFIA version 4 (dashed line). The agreement between the different calculations is very good. The small discrepancies (at higher frequencies mainly) can be explained by the gridding and possibly to some extent the different models for the losses. In MAFIA an equivalent conductivity of $\omega_0\varepsilon_0\varepsilon''$ with $\omega_0 = 2\pi 10^{10}$ is assumed. The MAFIA code is based on a finite integration time domain method, see [21, 22]. The code can only model normal incidence. Since MAFIA is based on a completely different method the agreement between the different calculations is a strong argument for the method and computer code developed here. The third curve in Figure 2 shows results measured on a test panel. The agreement is good considering the error sources of the measurements.

The measurements are performed on a square 600 × 600 mm test panel. The panel is placed between two horn antennas, each at a distance of approximately 500 mm from the slab, see Figure 3. The antennas are connected to a vector network analyzer. The purpose is to determine the transmission of the fundamental mode as if the slab was of infinite extent.

Due to the excitation of higher order modes in the slab, a surface wave propagates along the slab and reaches the edges where it is partially reflected and partially radiated into free space, interfering with the fundamental mode transmitted through the slab. In order to remove the disturbances caused by the reflections and radiating edges, a software time domain gating is performed. Measurements are performed at a number of frequencies, and the results are transformed to the time domain. In the time domain, the disturbances are identified as arriving considerably later than the transmitted fundamental mode. A gate is applied in the time domain to exclude the unwanted contributions and then the result is transformed back to the frequency domain. It is this gated curve that is shown in Figure 2. However, the time domain gating cannot entirely separate the different contributions why the disturbances to some extent still affect the measurements. Another source of error is presumably a slight curvature of the slab. Furthermore the slab is not illuminated by a plane wave of a specific direction but rather a spectrum of plane waves since horns with rather small apertures ($< 2\lambda$) are used. Near the edges the angle of incidence is so large that grating lobes could be excited. The directions of these grating lobes are such that they should not interfere with the measurement. The different angles of incidence cause e.g. the surface wave with wave vector $\boldsymbol{k}_{t;0,-1}$ to have a non discrete value, causing a 'smoothing' of the measured curve compared to the calculated. Antennas with larger apertures as in [18] could give a more accurate result. The error in the permittivity of the slab in the range of ±5%. A different ε in the calculations will cause a frequency shift of the curve.

In Figures 4 and 5 a plane wave is incident at an angle $\theta_{0,0} = 20°$ and $\varphi_{00} = 0°$. The frequency is scanned from 8 to 12 GHz. Calculated magnitudes for the transmission and reflection of the propagating modes are shown. A grating lobe occurs at frequencies larger than 9.9 GHz as can be seen in the figures. At 12 GHz the grating lobe angle is $\theta_{0,-1} = 50.3°$. (See illustration in Figure 6).

By numerical experiments it is found that a good result is obtained with surprisingly few modes. Although the slab is piecewise homogeneous, comparisons with a homogeneous slab are relevant. For a homogeneous slab with relative permittivity

ε, modes propagate when $k_0^2\varepsilon' - |\boldsymbol{k}_{t;mn}|^2 > 0$. For an inhomogeneous slab with low or moderate loss and a moderately large ε', the propagating modes are definitely enclosed by the circle given by $k_0^2\varepsilon_{est} - |\boldsymbol{k}_{t;mn}|^2 > 0$, where $\varepsilon_{est} = \max\{\varepsilon'(\boldsymbol{r})\}$ and $\boldsymbol{r}$ is given by $\{\boldsymbol{r} : \boldsymbol{r}_t \in \mathcal{I}, 0 \leq z \leq \ell\}$. By including the modes within the circle and the modes adjacent, a reasonable result is obtained. This seems to be true for electrically thin slabs also, although the evanescent modes have larger amplitudes when the object is thin and should affect the result more in that case. On the other hand, in the limit of an infinitely thin slab the propagator equals the identity operator. The behaviour is thus significantly different from that of a thin PEC screen. In the example here, modes $(0,0), (0,\pm1), (0,-2), (\pm1,\pm1),$ and $(\pm1,0)$ fall within the circle at 12 GHz. As mentioned, all modes with indices $|m|, |n| \leq 5$ are included in the example which is more than required in the scale used. The modes above $|m|, |n| \leq 3$ only give small contributions.

In section 2.3 it is mentioned that the coefficients given in (2.14) can be calculated using an entire domain basis (Appendix B). In general, a subdomain basis (e.g. pulse basis) is preferred though, especially when the object is piecewise homogeneous and Gibbs' phenomenon occurs in the entire domain representation of the permittivity. In that case a large number of basis functions is in general required to represent the material which results in a large number of Floquet modes.

3.2 Conductive slab

An infinite conductivity cannot be represented in the formulation presented here. However, large conductivities can be represented by a large imaginary part of the permittivity. Calculated results for a perforated lossy slab are shown in Figure 7. The cell is rectangular with $d_1 = 23.25$ mm and $d_2 = 15.55$ mm. The thickness is 1.1 mm and the relative permittivity $\varepsilon = 1 + i500$. There is one rectangular aperture per cell. The aperture size is 18.0 mm (along x) $\times$ 5.5 mm. A plane wave is incident at $\theta_{0,0} = 60°, \varphi_{00} = 90°$. Floquet modes with indices $|m|, |n| \leq 5$ are included. The permittivity is represented in the pulse basis (2.14). For TM transmission comparisons are made with a slab with the same geometry but consisting of a PEC (and calculated essentially by the method in [1]). The quantity $(\varepsilon'')^{\frac{1}{2}}\, t/\lambda_0$ where t is the thickness of the slab essentially determines an upper limit for the number of modes that can be included before the calculation of the propagator $\mathcal{K}$ becomes inaccurate and the matrix ill-conditioned. If the maximum number of modes that can be included is enough to represent the fields then the calculation gives a good result. In the example here the chosen value of ε'' corresponds to an effective conductivity of 280 S/m at 10 GHz which is far from say the conductivity of copper ($5.6 \cdot 10^7$ S/m) for which the PEC approximation is appropriate. For copper, the skin depth is 6.7μm at 10 GHz while the corresponding skin depth for $\varepsilon'' = 500$ is 0.3 mm. Although the skin depths differ by a factor of 450, the skin depth 0.3 mm is small compared to the length of the aperture which is why the shape of the curves for the transmitted TM polarised fundamental mode agree rather well. Obviously, a lot of absorption occurs in the skin.

Comparisons are relevant with homogeneous slabs regarding the decay of the

modes with respect to z. The decay is governed by the eigenvalues of the matrix $\mathcal{D}+\mathcal{C}$ for both inhomogeneous and homogeneous slabs. For a homogeneous medium with large losses ($\omega\varepsilon'' \gg \omega\epsilon'$), there is less difference between modes for which $\mathrm{Re}(k_0^2(\varepsilon'+i\varepsilon'')-|\boldsymbol{k}_{t;m,n}|^2)$ is larger or less than zero compared to a low loss medium. All modes are rapidly attenuated in the case of large losses. For a large loss medium (and a $+z$ wave direction) $\arg(k_{z;m,n})$ varies between $\pi/4-\mathcal{O}(\varepsilon'/\varepsilon'')$ and $\pi-\mathcal{O}(\varepsilon'/\varepsilon'')$ with increasing mode numbers $|m|$, $|n|$, (where $\mathcal{O}(x)<Cx$ when $x\to 0^+$ and C is a positive constant). The upper limit $\pi-\mathcal{O}(\varepsilon'/\varepsilon'')$ is not reached until $|\boldsymbol{k}_{t;m,n}|^2 \gg k_0^2\varepsilon''$ which happens for very large mode numbers $|m|$, $|n|$, when ε'' is large. Thus the simple guiding rule on how many modes to include suggested in section 3.1 is of no relevance for large losses.

In comparison, for a low loss medium $\arg(k_{z;m,n})$ varies between $\mathcal{O}(\varepsilon''/\varepsilon')$ and $\pi-\mathcal{O}(\varepsilon''/\varepsilon')$ with a distinctive jump from the lower to the upper limit when $\mathrm{Re}(k_0^2(\varepsilon'+i\varepsilon'')-|\boldsymbol{k}_{t;m,n}|^2)$ passes zero.

3.3 Pyramidal-shaped absorber-like metal backed structure

A pyramidal-shaped absorber-like structure is a $z-$dependent geometry that can be analyzed, see Figure 8. These types of structures are often used in e.g. anechoic chambers. The structure is backed by a PEC and thus the reflection coefficient is given by (2.31). The permittivity in this example is given by

$$\varepsilon(\boldsymbol{r}_t,z)=\begin{cases}\begin{cases}2.5+i & |x|\le 0.4z \text{ and } |y|\le 0.4z\\ 1 & \text{otherwise}\end{cases} & ,0\le z<30 \text{ mm}\\ 2.5+i & ,30\le z\le 42 \text{ mm}\end{cases} \tag{3.1}$$

Floquet modes with indices $|m|\le 2$, $|n|\le 3$ are included. The permittivity is represented in the pulse basis (2.14). The ODE system is solved with an implicit method. The magnitude of the reflection coefficients for the modes that are propagating in free space are shown in Figure 8 for an incident plane wave with $\theta_{0,0}=45°$, and $\varphi_{00}=0°$. A higher order mode with index $(0,-1)$ propagates in free space.

4 Concluding remarks

In this paper an analysis method for inhomogeneous dielectric frequency selective structures is derived. The structures that can be analyzed are periodic and inhomogeneous in the lateral directions. An arbitrary dependence is assumed in the longitudinal direction. The fields in the cell are expanded in a set of entire domain orthonormal vector basis functions. The constitutive parameter is expanded in local and entire domain basis respectively. The expansions are used to derive a set of coupled ODE:s for a propagator. A wave splitting physical in free space is then used to obtain the reflection and transmission matrices.

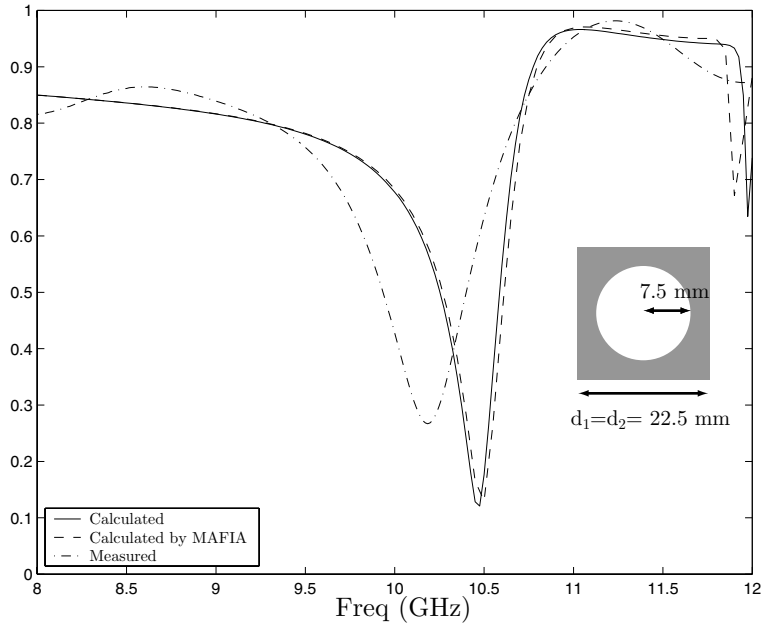

Figure 2: Magnitude of transmission for the fundamental mode, normal incidence with $\varphi_{00} = 0°$, $\varepsilon = 3.97 + i0.037$, slab thickness 5.1 mm, calculations compared with measurements (*cf.* Figure 6).

The permittivity is preferably expanded in a subdomain basis where a simple pulse basis is appropriate especially for a piecewise homogeneous case. An entire domain basis is also tried for the permittivity but found less successful.

The calculated results using the current method are, in a special case, compared with results obtained with a time domain based method and the agreement is very good. In the same case the results are compared with measurements; the agreement is good considering the sources of error in the measurements. Examples are given for a medium with small losses as well as very large losses. A metal backed pyramidal-shaped structure is also considered.

The method presented can easily be generalized to a medium with more complex constitutive relations.

Acknowledgment

The partial support by the Swedish Research Council for Engineering Sciences and CelsiusTech Electronics AB (Sweden) is gratefully acknowledged. The authors are also grateful to Ulf Dobson at Celsius Applied Composites AB, Ljungby, (Sweden) for help with the measurements and Joakim Olofsson at CelsiusTech Electronics AB for MAFIA comparisons.

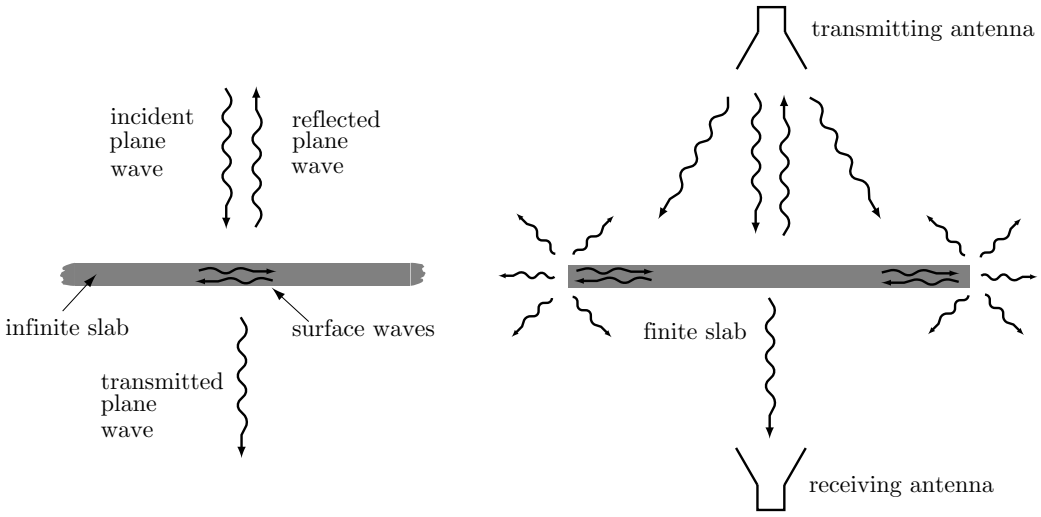

Figure 3: Ideal vs. actual test situation corresponding to example in section 3.1.

Appendix A Properties of the vector functions

$$\int_{\mathcal{I}} \boldsymbol{A}_{\tau mn}(\boldsymbol{r}_t) \cdot \boldsymbol{A}^*_{\tau' m' n'}(\boldsymbol{r}_t) dS = \delta_{\tau\tau'}\delta_{nn'}\delta_{mm'} \tag{A.1}$$

$$\nabla_t^2 \boldsymbol{A}_{\tau mn}(\boldsymbol{r}_t) = -k_{t;mn}^2 \boldsymbol{A}_{\tau mn}(\boldsymbol{r}_t)$$

$$\begin{aligned}
&\nabla \cdot \boldsymbol{A}_{1mn}(\boldsymbol{r}_t) = 0 \\
&\nabla \cdot \boldsymbol{A}_{2mn}(\boldsymbol{r}_t) = -k_{t;mn}\psi_{mn}(\boldsymbol{r}_t) \\
&\nabla \cdot \boldsymbol{A}_{3mn}(\boldsymbol{r}_t) = 0
\end{aligned}$$

$$\begin{aligned}
&\hat{z} \cdot \boldsymbol{A}_{\tau mn}(\boldsymbol{r}_t) = 0, \qquad \tau = 1, 2 \\
&\hat{z} \cdot \boldsymbol{A}_{3mn}(\boldsymbol{r}_t) = \psi_{mn}(\boldsymbol{r}_t) \\
&\hat{z} \times \boldsymbol{A}_{1mn}(\boldsymbol{r}_t) = \boldsymbol{A}_{2mn}(\boldsymbol{r}_t) \\
&\hat{z} \times \boldsymbol{A}_{2mn}(\boldsymbol{r}_t) = -\boldsymbol{A}_{1mn}(\boldsymbol{r}_t) \\
&\hat{z} \times \boldsymbol{A}_{3mn} = 0
\end{aligned}$$

$$\begin{aligned}
&\nabla \times \boldsymbol{A}_{1mn}(\boldsymbol{r}_t) = k_{t;mn}\boldsymbol{A}_{3mn}(\boldsymbol{r}_t) \\
&\nabla \times \boldsymbol{A}_{2mn}(\boldsymbol{r}_t) = 0 \\
&\nabla \times \boldsymbol{A}_{3mn}(\boldsymbol{r}_t) = k_{t;mn}\boldsymbol{A}_{1mn}(\boldsymbol{r}_t)
\end{aligned}$$

From these relations one easily obtain the orthogonality relations for the vector functions $\boldsymbol{u}_{\tau mn}$ and $\boldsymbol{v}_{\tau mn}$

$$\int\limits_{\mathcal{I} \text{ at } z=z_0} \boldsymbol{u}_{\tau mn} \cdot \boldsymbol{u}^*_{\tau' m' n'} dS = e^{-2\mathrm{Im}\gamma_{mn}k_0 z_0}\delta_{\tau\tau'}\delta_{mm'}\delta_{nn'}$$

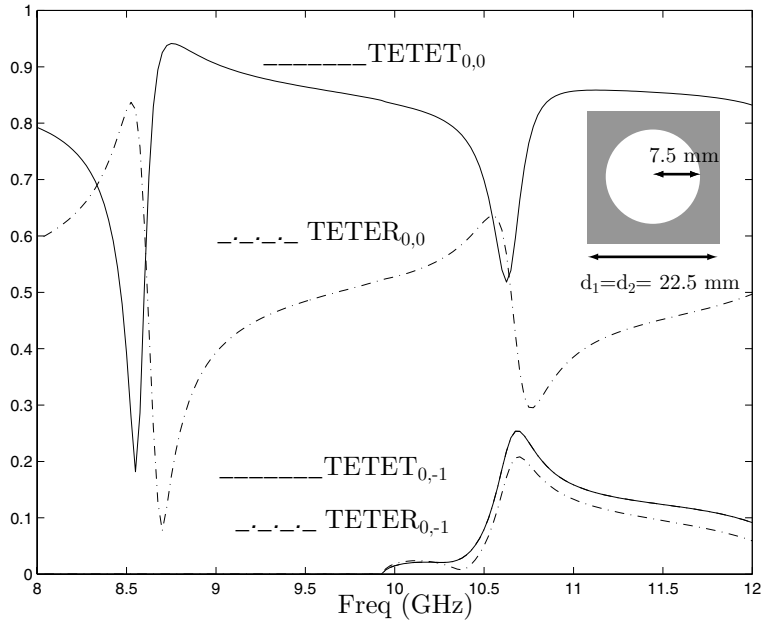

Figure 4: Magnitude of transmission and reflection coefficients of the propagating modes for the TE case (*cf.* Figure 6), $\varepsilon = 3.97 + i0.037$, slab thickness 5.1 mm, oblique incidence: $\theta_{0,0} = 20^\circ$ and $\varphi_{00} = 0^\circ$.

$$\int\limits_{\mathcal{I}\text{ at }z=z_0} \boldsymbol{v}_{\tau mn} \cdot \boldsymbol{v}^*_{\tau' m' n'} dS = e^{2\mathrm{Im}\gamma_{mn} k_0 z_0} \delta_{\tau\tau'} \delta_{mm'} \delta_{nn'}$$

$$\int\limits_{\mathcal{I}\text{ at }z=z_0} \boldsymbol{u}_{1mn} \times \boldsymbol{u}^*_{2m'n'} dS = ie^{-2\mathrm{Im}\gamma_{mn} k_0 z_0} \delta_{mm'} \delta_{nn'} (-\gamma^*_{mn} \hat{z} + \lambda_{mn} \hat{k}_{t;mn})$$

$$\int\limits_{\mathcal{I}\text{ at }z=z_0} \boldsymbol{u}_{2mn} \times \boldsymbol{u}^*_{1m'n'} dS = ie^{-2\mathrm{Im}\gamma_{mn} k_0 z_0} \delta_{mm'} \delta_{nn'} (-\gamma_{mn} \hat{z} + \lambda_{mn} \hat{k}_{t;mn})$$

$$\int\limits_{\mathcal{I}\text{ at }z=z_0} \boldsymbol{v}_{1mn} \times \boldsymbol{v}^*_{2m'n'} dS = ie^{2\mathrm{Im}\gamma_{mn} k_0 z_0} \delta_{mm'} \delta_{nn'} (-\gamma^*_{mn} \hat{z} + \lambda_{mn} \hat{k}_{t;mn})$$

$$\int\limits_{\mathcal{I}\text{ at }z=z_0} \boldsymbol{v}_{2mn} \times \boldsymbol{v}^*_{1m'n'} dS = ie^{2\mathrm{Im}\gamma_{mn} k_0 z_0} \delta_{mm'} \delta_{nn'} (-\gamma_{mn} \hat{z} + \lambda_{mn} \hat{k}_{t;mn})$$

$$\int\limits_{\mathcal{I}\text{ at }z=z_0} \boldsymbol{u}_{1mn} \times \boldsymbol{v}^*_{2m'n'} dS = ie^{i2\mathrm{Re}\gamma_{mn} k_0 z_0} \delta_{mm'} \delta_{nn'} (-\gamma^*_{mn} \hat{z} + \lambda_{mn} \hat{k}_{t;mn})$$

$$\int\limits_{\mathcal{I}\text{ at }z=z_0} \boldsymbol{u}_{2mn} \times \boldsymbol{v}^*_{1m'n'} dS = ie^{i2\mathrm{Re}\gamma_{mn} k_0 z_0} \delta_{mm'} \delta_{nn'} (-\gamma_{mn} \hat{z} + \lambda_{mn} \hat{k}_{t;mn})$$

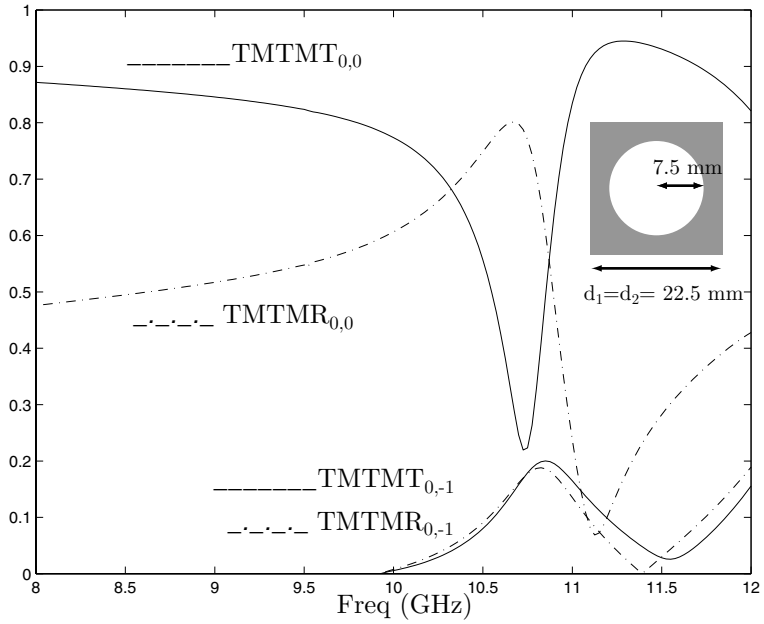

Figure 5: Magnitude of transmission and reflection coefficients of the propagating modes for the TM case (*cf.* Figure 6), $\varepsilon = 3.97 + i0.037$, slab thickness 5.1 mm, oblique incidence:$\theta_{0,0} = 20^\circ$ and $\varphi_{00} = 0^\circ$.

$$\int\limits_{\mathcal{I} \text{ at } z=z_0} \mathbf{v}_{1mn} \times \boldsymbol{u}^*_{2m'n'} dS = ie^{-i2\mathrm{Re}\gamma_{mn}k_0 z_0}\delta_{mm'}\delta_{nn'}(-\gamma^*_{mn}\hat{z} + \lambda_{mn}\hat{k}_{t;mn})$$

$$\int\limits_{\mathcal{I} \text{ at } z=z_0} \mathbf{v}_{2mn} \times \boldsymbol{u}^*_{1m'n'} dS = ie^{-i2\mathrm{Re}\gamma_{mn}k_0 z_0}\delta_{mm'}\delta_{nn'}(-\gamma_{mn}\hat{z} + \lambda_{mn}\hat{k}_{t;mn})$$

In the region $z < 0$, the electric field can be expressed as

$$\boldsymbol{E}(\boldsymbol{r}) = \boldsymbol{E}^i(\boldsymbol{r}) + \boldsymbol{E}^r(\boldsymbol{r})$$

where the incident field is given by

$$\boldsymbol{E}^i(\boldsymbol{r}) = \sum_{\tau=1}^{2}\sum_{m=-\infty}^{\infty}\sum_{n=-\infty}^{\infty} a_{\tau mn}\boldsymbol{u}_{\tau mn}(\boldsymbol{r}) \tag{A.2}$$

If the incident wave is a plane vector wave then

$$\boldsymbol{E}^i(\boldsymbol{r}) = a_{100}\boldsymbol{u}_{100}(\boldsymbol{r}) + a_{200}\boldsymbol{u}_{200}(\boldsymbol{r}) \tag{A.3}$$

Any plane wave with wave vector $\boldsymbol{k}_0$ can be obtained from this combination by suitable choices of a_{100} and a_{200}. The general incident field in equation (A.2) is relevant for a cascade of several periodic structures. The reflected field is given by

$$\boldsymbol{E}^r(\boldsymbol{r}) = \sum_{\tau=1}^{2}\sum_{m=-\infty}^{\infty}\sum_{n=-\infty}^{\infty} b_{\tau mn}\mathbf{v}_{\tau mn}(\boldsymbol{r}) \tag{A.4}$$

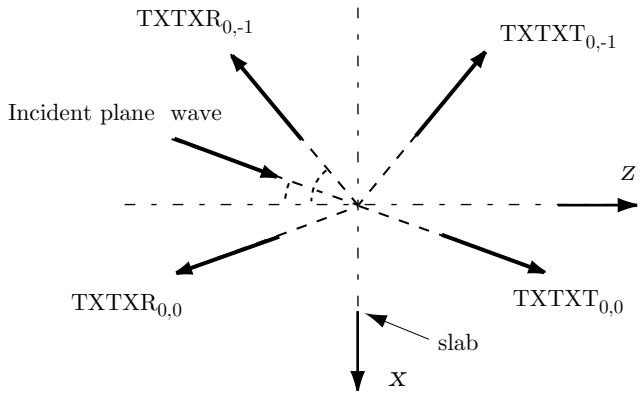

Figure 6: Propagating modes corresponding to Figures 4 and 5.

In the half space $z > \ell$ the electric field is expanded in forward going waves

$$\boldsymbol{E}^t(\boldsymbol{r}) = \sum_{\tau=1}^{2} \sum_{m=-\infty}^{\infty} \sum_{n=-\infty}^{\infty} f_{\tau mn} \boldsymbol{u}_{\tau mn}(\boldsymbol{r}) \tag{A.5}$$

Since

$$\boldsymbol{H}^i(\boldsymbol{r}) = -\frac{i}{\eta_0} \sum_{mn} a_{1mn} \boldsymbol{u}_{2mn} + a_{2mn} \boldsymbol{u}_{1mn}$$

$$\boldsymbol{H}^r(\boldsymbol{r}) = \frac{i}{\eta_0} \sum_{mn} b_{1mn} \boldsymbol{v}_{2mn} + b_{2mn} \boldsymbol{v}_{1mn}$$

it is seen that

$$\begin{aligned}
&\mathrm{Re} \int_{\mathcal{I} \text{ at } z=z_0} \boldsymbol{E}^i \times \boldsymbol{H}^{i*} \cdot \hat{z} dS = \frac{1}{\eta_0} \sum_{mn} \mathrm{Re}\left(\gamma_{mn} e^{-2\mathrm{Im} k_{zmn} z_0}\right) \left(|a_{1mn}|^2 + |a_{2mn}|^2\right) \\
&\mathrm{Re} \int_{\mathcal{I} \text{ at } z=z_0} \boldsymbol{E}^r \times \boldsymbol{H}^{r*} \cdot \hat{z} dS = -\frac{1}{\eta_0} \sum_{mn} \mathrm{Re}\left(\gamma_{mn} e^{2\mathrm{Im} k_{zmn} z_0}\right) \left(|b_{1mn}|^2 + |b_{2mn}|^2\right) \\
&\int_{\mathcal{I} \text{ at } z=z_0} \boldsymbol{E}^i \times \boldsymbol{H}^{r*} \cdot \hat{z} dS = -\frac{1}{\eta_0} \sum_{mn} \left(a_{1mn} b_{1mn}^* \gamma_{mn}^* + a_{2mn} b_{2mn}^* \gamma_{mn}\right) e^{2i\mathrm{Re} k_{zmn} z_0} \\
&\int_{\mathcal{I} \text{ at } z=z_0} \boldsymbol{E}^r \times \boldsymbol{H}^{i*} \cdot \hat{z} dS = \frac{1}{\eta_0} \sum_{mn} \left(b_{1mn} a_{1mn}^* \gamma_{mn}^* + b_{2mn} a_{2mn}^* \gamma_{mn}\right) e^{-2i\mathrm{Re} k_{zmn} z_0} \\
&\mathrm{Re} \int_{\mathcal{I} \text{ at } z=z_1} \boldsymbol{E}^t \times \boldsymbol{H}^{t*} \cdot \hat{z} dS = \frac{1}{\eta_0} \sum_{mn} \mathrm{Re} \gamma_{mn} e^{-2\mathrm{Im} k_{zmn} z_1} |f_{1mn}|^2
\end{aligned} \tag{A.6}$$

The divergence theorem gives

$$\mathrm{Re} \int_{\mathcal{I} \text{ at } z=z_0} (\boldsymbol{E}^i + \boldsymbol{E}^r) \times (\boldsymbol{H}^{i*} + \boldsymbol{H}^{r*}) \cdot \hat{z} dS = \mathrm{Re} \int_{\mathcal{I} \text{ at } z=z_1} (\boldsymbol{E}^t \times \boldsymbol{H}^{t*}) \cdot \hat{z} dS$$

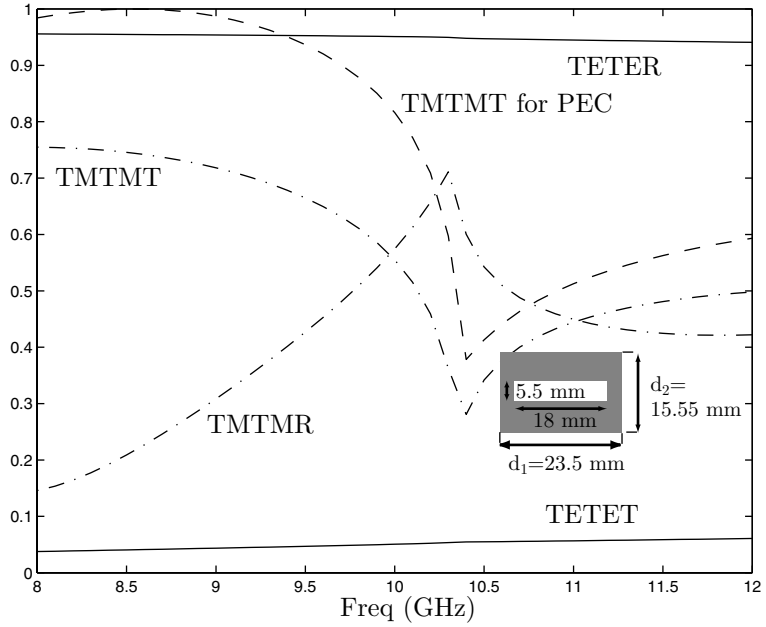

Figure 7: Magnitude of transmission and reflection coefficients of the fundamental modes for a perforated lossy slab with $\varepsilon = 1 + i500$ and slab thickness 1.1 mm, comparisons with a perfect electric conductor (PEC), oblique incidence:$\theta_{0,0} = 60^\circ$ and $\varphi_{00} = 90^\circ$.

The energy relation then follows from the relations in Eq. (A.6)

$$\begin{aligned}\sum_{\tau mn} \mathrm{Re}(\gamma_{mn} e^{-2\mathrm{Im}k_{zmn}z_0})|a_{\tau mn}|^2 - \sum_{\tau mn} \mathrm{Re}(\gamma_{mn} e^{-2\mathrm{Im}k_{zmn}z_1})|f_{\tau mn}|^2 \\ - \sum_{\tau mn} \mathrm{Re}(\gamma_{mn} e^{2\mathrm{Im}k_{zmn}z_0})|b_{\tau mn}|^2 \\ = 2(-1)^{\tau-1} \sum_{\tau mn} \mathrm{Im}\,(\gamma_{mn})\,\mathrm{Im}\left(a_{\tau mn} b^*_{\tau mn} e^{2i\mathrm{Re}k_{zmn}z_0}\right)\end{aligned}$$

When the surrounding medium is lossless the left hand side is a summation over the propagating modes and the right hand side is a summation over non-propagating modes. Since the periodic structure is embedded in vacuum in this paper it is seen that

$$\delta_{mm'}\delta_{nn'} - \sum_{m''n''} \Gamma_{mn,m''n''}\Gamma^*_{m''n'',m'n'} - \sum_{m''n''} \mathcal{T}^\dagger_{mn,m''n''}\mathcal{T}_{m''n'',m'n'} = 0 \qquad (A.7)$$

where † denotes Hermite conjugate and the summation is over the propagating mode indices. It is also seen that

$$\mathrm{Im}\Gamma_{mn,m'n'} = 0 \qquad (A.8)$$

for mode indices mn corresponding to non-propagating modes.

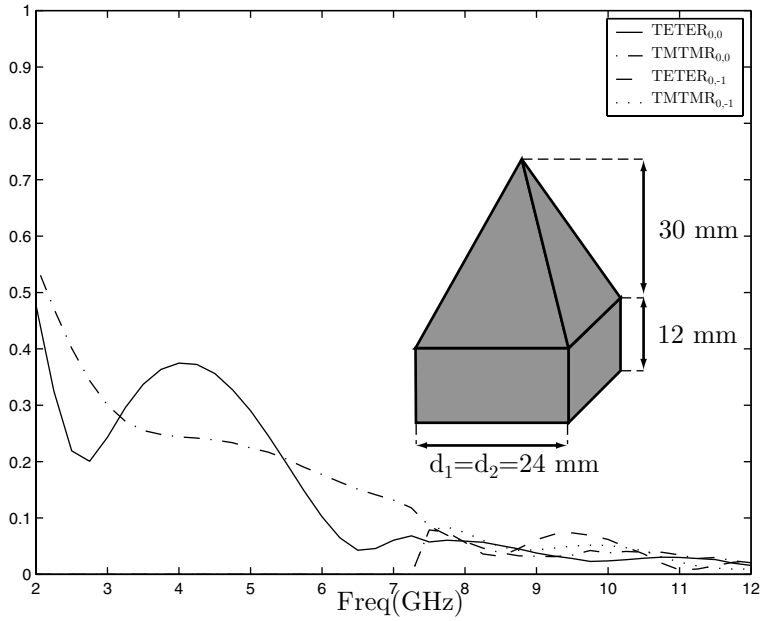

Figure 8: Magnitude of reflection coefficients for in free space propagating modes for a metal-backed lossy pyramidal-shaped structure with $\varepsilon = 2.5 + i$, oblique incidence: $\theta_{0,0} = 45^\circ$ and $\varphi_{00} = 0^\circ$.

Appendix B Expansion coefficients for the constitutive parameters in the entire domain basis

The integrals in Eq. (2.13) can be handled in some different ways. One way is to expand $\varepsilon(\boldsymbol{r}) - 1$ and $(\varepsilon(\boldsymbol{r}))^{-1} - 1$ as

$$\varepsilon(\boldsymbol{r}) - 1 = \sum_{mn} c_{mn}(k_0 z)\eta_{mn}(\boldsymbol{r}_t)$$
$$(\varepsilon(\boldsymbol{r}))^{-1} - 1 = \sum_{mn} f_{mn}(k_0 z)\eta_{mn}(\boldsymbol{r}_t)$$

cf. Eq. (2.1). Thus

$$\alpha_{12}(z) = \sum_{m''n''} c_{m''n''}(z) \int_{\mathcal{I}} \eta_{m''n''}(\boldsymbol{r}_t)\boldsymbol{A}^*_{2mn}(\boldsymbol{r}_t) \cdot \boldsymbol{A}_{2m'n'}(\boldsymbol{r}_t)\, dS$$
$$\alpha_{13}(z) = \sum_{m''n''} c_{m''n''}(z) \int_{\mathcal{I}} \eta_{m''n''}(\boldsymbol{r}_t)\boldsymbol{A}^*_{2mn}(\boldsymbol{r}_t) \cdot \boldsymbol{A}_{1m'n'}(\boldsymbol{r}_t)\, dS$$
$$\alpha_{21}(z) = \sum_{m''n''} f_{m''n''}(z)\lambda_{mn}\lambda_{m'n'} \int_{\mathcal{I}} \eta_{m''n''}(\boldsymbol{r}_t)\boldsymbol{A}^*_{3mn}(\boldsymbol{r}_t) \cdot \boldsymbol{A}_{3m'n'}(\boldsymbol{r}_t)\, dS$$

$$\alpha_{42}(z) = -\sum_{m''n''} c_{m''n''}(z) \int_{\mathcal{I}} \eta_{m''n''}(\boldsymbol{r}_t) \boldsymbol{A}^*_{1mn}(\boldsymbol{r}_t) \cdot \boldsymbol{A}_{2m'n'}(\boldsymbol{r}_t)\, dS$$

$$\alpha_{43}(z) = -\sum_{m''n''} c_{m''n''}(z) \int_{\mathcal{I}} \eta_{m''n''}(\boldsymbol{r}_t) \boldsymbol{A}^*_{1mn}(\boldsymbol{r}_t) \cdot \boldsymbol{A}_{1m'n'}(\boldsymbol{r}_t)\, dS$$

and these are reduced to

$$\alpha_{12}(z) = \hat{k}_{t;mn} \cdot \hat{k}_{t;m'n'} \sum_{m''n''} c_{m''n''}(z) \mathcal{W}_{mnm'n'm''n''}$$

$$\alpha_{13}(z) = \hat{z} \cdot (\hat{k}_{t;mn} \times \hat{k}_{t;m'n'}) \sum_{m''n''} c_{m''n''}(z) \mathcal{W}_{mnm'n'm''n''}$$

$$\alpha_{21}(z) = \lambda_{mn}\lambda_{m'n'} \sum_{m''n''} f_{m''n''}(z) \mathcal{W}_{mnm'n'm''n''}$$

$$\alpha_{42}(z) = \alpha_{13}(z)$$

$$\alpha_{43}(z) = -\alpha_{12}(z)$$

The matrix $\mathcal{W}$ reads

$$\begin{aligned} \mathcal{W}_{mnm'n'm''n''} &= \int_{\mathcal{I}} \eta^*_{mn}(\boldsymbol{r}_t) \eta_{m'n'}(\boldsymbol{r}_t) \eta_{m''n''}(\boldsymbol{r}_t)\, dS \\ &= \frac{1}{\sqrt{D}} \delta_{m,m'+m''} \delta_{n,n'+n''} \end{aligned}$$

Thus

$$\alpha_{12}(z) = \frac{1}{\sqrt{D}}\, \hat{k}_{t;mn} \cdot \hat{k}_{t;m'n'}\, c_{m-m',n-n'}(z) = -\alpha_{43}$$

$$\alpha_{13}(z) = \frac{1}{\sqrt{D}}\, \hat{z} \cdot (\hat{k}_{t;mn} \times \hat{k}_{t;m'n'})\, c_{m-m',n-n'}(z) = \alpha_{42}$$

$$\alpha_{21}(z) = \frac{1}{\sqrt{D}}\, \lambda_{mn}\lambda_{m'n'}\, f_{m-m',n-n'}(z)$$

References

[1] R. Petit (ed.). *Electromagnetic Theory of Gratings.* Springer Verlag, Berlin, 1980.

[2] T. K. Wu (ed.). *Frequency Selective Surface and Grid Array.* John Wiley, New York, 1995.

[3] B. A. Munk. *Frequency Selective Surfaces: Theory and Design.* John Wiley, New York, 2000.

[4] J. C. Vardaxoglou. *Frequency Selective Surfaces — Analysis and Design.* Research Studies Press, England, 1997.

[5] R. Mittra, T. Cwik and C. H. Chan. Techniques for analyzing frequency selective surfaces—a review. *Proceedings of the IEEE*, **76**(12), 1593–1615, 1988.

[6] F. S. Johanssson. Analysis and design of double-layer frequency selective surfaces *IEE Proceedings part H*, **132**(5), 319–325, 1985.

[7] E. L. Pelton and B. A. Munk. A streamlined metallic radome. *IEEE Transactions on Antennas and Propagation*, **22**, 799–803, 1974.

[8] S. Poulsen. Scattering from frequency selective surfaces: A continuity condition for entire domain basis functions and an improved set of basis functions for crossed dipoles. *IEE Proceedings-Microwawes, Antennas and Propagation*, **146**(3), 234–240, 1999.

[9] B. Widenberg, S. Poulsen, A. Karlsson. Scattering from Thick Frequency Selective Screens. *Journal of Electromagnetic Waves and Applications*, **14**, 1301–1327, 2000.

[10] T. F. Eibert, J. L. Volakis, D. L. Wilton and D. R. Jackson. Hybrid FE/BI Modeling of 3-D Doubly Periodic Structures Utilizing Triangular Prismatic Elements and an MPIE Formulation Accelerated by the Ewald Transformation. *IEEE Transactions on Antennas and Propagation*, **47**(5), 843–850, 1999.

[11] D. T. McGrath and V. P. Pyati Periodic structure analysis using a hybrid finite element method. *Radio Science*, **31**(5), 1173–1179, 1996.

[12] S. He. Wave-splitting approach to a scattering problem for a laterally periodic inhomogeneous structure. *Journal of Electromagnetic Waves and Applications*, **11**(5), 633–644, 1997.

[13] O. Forslund and S. He. Electromagnetic scattering from an inhomogeneous grating using a wave-splitting approach. *Progress in Electromagnetics Research, PIER 19*, 147–171, 1998.

[14] B. Jakoby, A.-R. Baghai-Wadji. Analysis of Bianisotropic Layered Structures with laterally Periodic Inhomogeneities—An Eigenoperator Formulation. *IEEE Transactions on Antennas and Propagation*, **44**(5), 615–626, 1996.

[15] S. T. Peng, T. Tamir and H. L. Bertoni. Theory of periodic dielectric waveguides *IEEE Transactions on Microwave Theory and Techniques*, **23**(1), 123–133, 1975.

[16] H. L. Bertoni, L. S. Cheo and T. Tamir. Frequency-selective reflection and transmission by a periodic dielectric layer. *IEEE Transactions on Antennas and Propagation*, **37**(1), 78–83, 1989.

[17] J. C. W. A. Costa and A. J. Giarola. Analysis of the selective behaviour of multilayer structures with a dielectric grating. *IEEE Transactions on Microwave Theory and Techniques*, **43**(5), 529–533, 1995.

[18] S. Tibuleac, R. Magnusson, T. A. Maldonado, P. P. Young and T. R. Holzheimer. Dielectric Frequency-Selective Structures Incorporating Waveguide Gratings. *IEEE Transactions on Microwave Theory and Techniques*, **48**(4), 553–561, 2000.

[19] H. Ammari and S. He. Homogenization and scattering for gratings. *Journal of Electromagnetic Waves and Applications*, **11**(12), 1669–1683, 1997.

[20] S. Rikte, M. Andersson and G. Kristensson. Homogenization of woven materials. *International Journal of Electronics and Communications, Archiv für Electronik und Übertragungstechnik, AEÜ* , **53**(5), 261–271, 1999.

[21] M. Clemens, R. Schuhmann, U. v. Rienen and T. Weiland. Modern Krylov Subspace Methods in Electromagnetic Field Computations Using the Finite Integration Theory. *Applied Computational Electromagnetics Society Journal*, **11**(1), 70–84, 1996.

[22] T. Weiland, M. Bartsch, U. Becker, M. Bihn, U. Blell, M. Clemens, M. Dehler, M. Dohlus, M. Drevlak, X. Du, R. Ehmann, A. Eufinger, S. Gutschling, P. Hahne, R. Klatt, B. Krietenstein, A. Langstrof, P. Pinder, O. Podebrad, T. Pröpper, U. v. Rienen, D. Schmidt, R. Schuhmann, A. Schulz, S. Schupp, P. Schütt, P. Thoma, M. Timm, B. Wagner, R. Weber, S. Wipf, H. Wolter and Z. Min. MAFIA Version 4. *Proceedings of the Computational Accelerator physics Conference (CAP)*, 1996, Williamsburg, Virginia, 65–70.

[23] B. Baekelandt, F. Olyslager and D. De Zutter. Low-Frequency Reflectivity Approximation for Two- and Three-Dimensional EM Absorbers. *IEEE Transactions on Electromagnetic Compatibility*, **41**(4), 354–360, 1999.